Photochemistry and Photobiology, 2000, 72(1): 62–74

Damage to DNA in Bacterioplankton: A Model of Damage by Ultraviolet Radiation and its Repair as Influenced by Vertical Mixing¶

Yannick Huot*[1], Wade H. Jeffrey[2], Richard F. Davis[1] and John J. Cullen[1]

[1]Center for Environmental Observation Technology and Research, Department of Oceanography, Dalhousie University, Halifax, NS, Canada and
[2]Center for Environmental Diagnostics and Bioremediation, University of West Florida, Pensacola, FL

Received 3 March 2000; accepted 24 April 2000

ABSTRACT

A model of UV-induced DNA damage in oceanic bacterioplankton was developed and tested against previously published and novel measurements of cyclobutane pyrimidine dimers (CPD) in surface layers of the ocean. The model describes the effects of solar irradiance, wind-forced mixing of bacterioplankton and optical properties of the water on net DNA damage in the water column. The biological part includes the induction of CPD by UV radiation and repair of this damage through photoreactivation and excision. The modeled damage is compared with measured variability of CPD in the ocean: diel variation in natural bacterioplankton communities at the surface and in vertical profiles under different wind conditions (net damage as influenced by repair and mixing); *in situ* incubation of natural assemblages of bacterioplankton (damage and repair, no mixing); and *in situ* incubation of DNA solutions (no repair, no mixing). The model predictions are generally consistent with the measurements, showing similar patterns with depth, time and wind speed. A sensitivity analysis assesses the effect on net DNA damage of varying ozone thickness, colored dissolved organic matter concentration, chlorophyll concentration, wind speed and mixed layer depth. Ozone thickness and mixed layer depth are the most important factors affecting net DNA damage in the mixed layer. From the model, the total amplification factor (TAF; a relative measure of the increase of damage associated with a decrease in ozone thickness) for net DNA damage in the euphotic zone is 1.7, as compared with 2.1–2.2 for irradiance weighted for damage to DNA at the surface.

INTRODUCTION

Ultraviolet radiation (UVR)† is a significant ecological factor in aquatic ecosystems (1,2); it damages DNA (3,4), inhibits photosynthesis (5) and produces many other biological and chemical effects (6,7). Sessile organisms in clear, shallow waters (8,9) and plankton (7,10,11), due to their small size and epipelagic niche, are particularly susceptible to UVR.

Planktonic bacteria are an important component of aquatic ecosystems, playing major roles in the cycling of nitrogen (12), carbon and other nutrients (13). Estimated bacterial productivity varies between 14 and 76% of primary productivity, depending on the time of year and location (as reviewed by Jeffrey *et al.* [14]) and, in oligotrophic waters, their biomass is of the same order as that of phytoplankton (15).

The effects of UVR on bacterioplankton have received considerable attention in recent years (reviewed in Jeffrey *et al.* [11]). Conceptual models describe the direct effect of UVR on bacterioplankton and the mitigating influence of mixing on the balance between DNA damage and repair on bacterioplankton (16,17, see also Gieskes and Buma [18]). The interacting photochemical and microbiological influences of UVR-absorbing colored dissolved organic matter (CDOM) have also been addressed in conceptual models (19,20) and in recent field and laboratory studies (as discussed by Pausz and Herndl [21]). These complex interactions between physical, biological, photochemical and chemical processes can be addressed quantitatively with numerical models (*e.g.* [22,23–26]). To begin this process, we use a numerical model to simulate net DNA damage in bacterioplankton as influenced by optical, physical and biological variability. The model describes damage and repair processes (photoreactivation and excision repair) as influenced by variable spectral irradiance during vertical mixing of bacterioplankton in the upper water column.

We focus on DNA because UVR-induced damage to DNA can lead to reduced physiological activity (*e.g.* measured as thymidine or leucine incorporation [27,28]) and eventual death of bacteria in the upper water column. Ver-

¶Posted on the web on 5 May 2000.
*To whom correspondence should be addressed at: CEOTR, Department of Oceanography, Dalhousie University, Halifax, NS, B3H 4J1, Canada. Fax: 902-494-2039; e-mail: yhuot@is2.dal.ca
†*Abbreviations:* A, adenine; C, cytosine; CDOM, colored dissolved organic matter; CPD, cyclobutane pyrimidine dimer; DOM, dissolved organic matter; DU, Dobson unit; G, guanine; MAA, mycosporine-like amino acid; PAR, photosynthetically available radiation; PUR, photosynthetically usable radiation; RAF, radiation amplification factor; T, thymine; TAF, total amplification factor; TOMS, total ozone mapping spectrometer; UVA, 320–400 nm radiation; UVB, 280–320 nm radiation; UVR, ultraviolet radiation; UVT, ultraviolet transparent.

Table 1. Notation

Symbol	Interpretation	Units
a	Proportionality constant	Dimensionless
C_1	''Half saturation'' constant of excision repair function	CPD Mbp^{-1}
C_2	Steepness of ascent of excision repair function	CPD^{-1} Mbp
C_3	Position of threshold in the excision repair function	CPD Mbp^{-1}
DOM	DOM concentration in water	g m^{-3}
$E_d(z, \lambda, t)$	Downwelling spectral irradiance	W m^{-2} nm^{-1}
$E_u(z, \lambda, t)$	Upwelling spectral irradiance	W m^{-2} nm^{-1}
$E_o(z, \lambda, t)$	Scalar irradiance	W m^{-2} nm^{-1}
$E^*_{DNA}(E)$	Irradiance weighted for DNA damage	CPD Mbp^{-1} s^{-1}
$E^*_{PR}(E)$	Irradiance weighted for photoreactivation	s^{-1}
$E_{diff}(z, \lambda, t)$	Diffuse downwelling spectral irradiance	W m^{-2} nm^{-1}
$E_{dir}(z, \lambda, t)$	Direct downwelling spectral irradiance	W m^{-2} nm^{-1}
$J_{dam}(E)$	DNA-specific rate of damage	CPD Mbp^{-1} s^{-1}
$J_{PR}(E, N)$	DNA-specific rate of photoreactivation repair	CPD Mbp^{-1} s^{-1}
$J_{ER}(N)$	DNA-specific rate of excision repair	CPD Mbp^{-1} s^{-1}
$j(t)$	Underwater solar zenith angle	Degrees
k_1	Rate of binding of the photolyase enzyme	CPD^{-1} Mbp s^{-1}
$k_2(E)$	Specific rate of conversion of CPD to base pairs	s^{-1}
k_3	Maximum rate of CPD excision repair	CPD Mbp^{-1} s^{-1}
$K_{chl}(\lambda)$	Diffuse attenuation coefficient due to chlorophyll	m^{-1}
$K_d(\lambda)$	Diffuse attenuation coefficient for downwelling irradiance	m^{-1}
$K_{DOM}(\lambda)$	Diffuse attenuation coefficient due to CDOM	m^{-1}
K_z	Coefficient of Eddy diffusivity	m^2 s^{-1}
$K_w(\lambda)$	Attenuation coefficient due to water	m^{-1}
$\bar{N}$	DNA specific concentration of dimers	CPD Mbp^{-1}
$\bar{N}_{Euph}$	Average DNA-specific concentration of dimers in the euphotic zone.	CPD Mbp^{-1}
$\bar{N}_{mix}$	Average DNA-specific concentration of dimers in the mixed layer	CPD Mbp^{-1}
$\bar{N}_{submix}$	Average DNA-specific concentration of dimers below the mixed layer (to the euphotic zone depth)	CPD Mbp^{-1}
P	DNA-specific concentration of photolyase	Molecules Mbp^{-1}
PN	DNA-specific concentration of photolyase–CPD complex	CPD Mbp^{-1} or Molecules Mbp^{-1}
t	Time	s
z	Depth	m
z_{Euph}	Depth of the euphotic zone (defined as 1% of surface PUR)	m
z_{mix}	Depth of the mixed layer	m
$\epsilon_{DNA}(\lambda)$	Action spectrum for DNA damage	CPD Mbp^{-1} $(J\ m^{-2})^{-1}$
$\epsilon_{PR}(\lambda)$	Action spectrum for photoreactivation	$(J\ m^{-2})^{-1}$
λ	Wavelength	nm
$\bar{\mu}_d$	Average cosine for downwelling irradiance	Dimensionless

tical mixing is included because damage to DNA is caused mostly by short, rapidly attenuated UVB radiations (280–320 nm), while repair, through photoreactivation, depends on longer, more penetrating UVA (320–400 nm) and visible wavelengths. Consequently, mixing influences relative exposures to UVB *vs* longer wavelengths, and hence, the balance between damage and repair (17,18). Our model is evaluated through direct comparisons with published measurements from surface layers of the ocean (29) and new measurements of DNA damage from the Antarctic.

Consistent with qualitative models, our numerical simulations describe the temporal and vertical patterns of cyclobutane pyrimidine dimers (CPD) measured in the field. However, some parameters of the model are poorly constrained by laboratory measurements, so its predictive capability is limited. We interpret the results focusing on bacterioplankton, but, with care, they could be extended to any unshielded planktonic organisms, such as viruses and small phytoplankton.

MATERIALS AND METHODS

The model describes irradiance, mixing and biological responses to UVR. Its implementation can be summarized in five steps. (1) Initialization: before sunrise, 2000 virtual bacteria are distributed evenly in a mixed layer and, when the mixed layer depth (z_{mix}, m; see Table 1 for notation) is greater than the euphotic depth (z_{Euph}, m), 100 bacteria are distributed evenly between z_{mix} and z_{Euph}. (2) Irradiance model: at 5 min intervals throughout the day, spectral scalar irradiance is calculated through the water column. (3) Biological model: separate action spectra are used to weight irradiance for DNA damage (formation of dimers) and for photoreactivation. Weighted exposures for each 5 min interval are applied to the bacteria at their respective depths. Excision repair is calculated concurrently and depends solely on the concentration of dimers. (4) Mixing model: bacteria in the mixed layer are moved according to a random walk model, simulating vertical displacement over a 5 min interval. (5)

Time loop: a loop to step 2 is made every 5 min throughout the day until sunset. Then, all variables are saved for future use.

The irradiance model. Following the approach of Neale *et al.* (23), we used the model of Gregg and Carder (30) extended into the UV by Arrigo (24) to obtain downwelling spectral irradiance just below the sea surface ($E_d(0^-, \lambda, t)$, W m^{-2} nm^{-1}), where λ is the wavelength (nm) and t is the time (s). This formulation takes into account the latitude, time of day, time of year, ozone thickness, atmospheric water content, wind speed, air mass type and visibility. Sea surface reflection is calculated using Fresnel's law for flat sea surfaces; for rough surfaces, an empirical function of wind speed and solar zenith angle is used (30). Scalar irradiance ($E_o(0^-, \lambda, t)$, W m^{-2} nm^{-1}) is obtained through the relationship,

$$E_o(0^-) \approx E_d(0^-)/\bar{\mu}_d,$$

which assumes that upwelling irradiance (E_u) is negligible (*i.e.* $E_u \ll E_d$). The average cosine of the downwelling irradiance ($\bar{\mu}_d$, dimensionless) was obtained by using a more explicit version of the relationship proposed by Prieur and Sathyendranath (31) between $\bar{\mu}_d$, the underwater solar zenith angle (j, degrees; calculated from zenith angle and refraction), the ratio of direct to total downwelling irradiance just above sea surface ($E_{dir}/E_d(0^+)$) and the ratio of diffuse to total downwelling irradiance ($E_{diff}/E_d(0^+)$):

$$\frac{1}{\bar{\mu}_d(t)} = \frac{E_{dir}(0^+, t)/E_d(0^+, t)}{\cos j} + \frac{E_{diff}(0^+, t)/E_d(0^+, t)}{0.859}. \quad (1)$$

The subsurface scalar irradiance was propagated through the water column using Beer's law for diffuse irradiance (*e.g.* [32]):

$$E_o(z, \lambda) = E_o(0^-, \lambda) \cdot e^{-K_d(\lambda) \cdot z}, \quad (2)$$

where $K_d(\lambda)$, the downwelling diffuse attenuation coefficient (m^{-1}), is assumed constant with depth, z (m).

The diffuse attenuation coefficient includes contributions from the colored (CDOM) portion of dissolved organic matter (DOM) (K_{DOM}, m^{-1}) and chlorophyll (K_{chl}, m^{-1}), which are added to the attenuation coefficient for clear oceanic waters (K_w, m^{-1}) (33,34):

$$K_d(\lambda) = K_w(\lambda) + K_{DOM}(\lambda) + K_{chl}(\lambda). \quad (3)$$

Following Høerjslev (cited in Baker and Smith [33]), K_{DOM} is modeled assuming a constant ratio of CDOM attenuation to DOM concentration and an exponential decrease with wavelength:

$$K_{DOM}(\lambda) = 0.565 \cdot DOM \cdot e^{(-0.014 \cdot [\lambda - 380])}, \quad (4)$$

where *DOM* is the concentration of DOM in the water (g m^{-3}). Diffuse attenuation by chlorophyll was obtained by regression of $K_d(\lambda)$ *vs* chlorophyll (33). As a result, it includes contributions from chlorophyll and all covarying matter.

The depth of the euphotic zone (z_{Euph}) was approximated as the depth of 1% midday surface photosynthetically usable radiation (PUR, $E_{oPUR}(0^-)$, W m^2). The PUR (35) was calculated by weighting irradiance with a normalized absorption spectrum characteristic of microplankton (Ciotti *et al.*, in preparation).

The mixing model. Random walk models have been used extensively to simulate turbulent mixing processes in aquatic systems (*e.g.* [23,36,37–40]) with the movements of particles described as a function of eddy diffusivity (K_z, m^2 s^{-1}). We use the formulation proposed by Visser (41) for the random walk model but we use a diffusivity profile decreasing as $z^{-1/2}$ with depth (38, see also Franks and Marra [39]), which is consistent with wind forcing. The formulation of Visser (41) solves the problem encountered in previous models where small, neutrally buoyant particles accumulated in regions of low diffusivity (42,43). The drag coefficient was calculated as a function of wind speed using the relationship given by Large *et al.* (44).

The biological model. This model describes UVR-induced production of CPD and the repair of this damage by excision repair and photoreactivation.

Modeling the rate of DNA damage. We model the DNA-specific [per megabase pair (Mbp)] concentration of dimers in the bacteria ($N(t)$; CPD Mbp^{-1}) by assuming linearity between exposure and response (consistent with cumulative, one-hit kinetics at low concentrations of dimers). It follows that the DNA-specific rate of formation of pyrimidine dimers ($J_{dam}(t)$; CPD Mbp^{-1} s^{-1}) is described as a linear function of weighted irradiance (45):

$$J_{dam}(t) = E^*_{DNA}(t) = \int_{290}^{400} E_o(\lambda, t) \cdot \epsilon_{DNA}(\lambda)\, d\lambda. \quad (5)$$

Where $E^*_{DNA}(t)$ is irradiance weighted for DNA-specific damage (CPD Mbp^{-1} s^{-1}) at time t and $\epsilon_{DNA}(\lambda)$ is a spectral weighting function for CPD production (CPD Mbp^{-1} [J m^{-2}]$^{-1}$). This formulation for weighted irradiance allows direct calculation of DNA damage in absolute units.

An action spectrum for the T7 bacteriophage (46) is used for $\epsilon_{DNA}(\lambda)$ (Fig. 1a). It represents unshielded DNA (47,48), and assumes that the path length required for effective shielding by any UVR-absorbing compound is longer than the size of bacterial cells (49), consistent with results in bacterioplankton (50). To assess the effect of shielding by cellular material, an action spectrum for CPD induction in alfalfa seedlings (48) is used (Fig. 1a).

Photoreactivation repair. This is an enzymatic process mediated by light. The DNA-specific rate of photoreactivation ($J_{PR}(E, N)$, CPD Mbp^{-1} s^{-1}) can be controlled at low irradiance by available light and at high irradiance by the binding rate between enzyme and substrate. Assuming steady-state and constant enzymatic rates over each time step, we use the Michaelis–Menten relationship to model this process:

$$J_{PR}(E, N) = \frac{dPN}{dt} = a \cdot k_2(E) \cdot \left[\frac{k_1 \cdot P \cdot N(t)}{k_2(E) + k_1 \cdot N(t)}\right], \quad (6)$$

where PN is the concentration of enzyme–dimer complexes (CPD Mbp^{-1} or molecules Mbp^{-1}); $k_2(E)$ is an irradiance-dependent maximum rate of repair (*i.e.* rate for the reversal of dimers [s^{-1}]); k_1 is the rate of binding between the enzyme and the dimer (CPD^{-1} Mbp s^{-1}), set to 8.3×10^{-3} CPD^{-1} Mbp s^{-1} (51) assuming 4.6 Mbp cell^{-1} (52); P is the concentration of photolyase enzyme (molecule Mbp^{-1}), taken equal to 4 (51) assuming again 4.6 Mbp cell^{-1}; and $N(t)$ is the concentration of dimers (CPD Mbp^{-1}). A scaling factor, a (unitless), is set to 0.1, to reduce predicted rates. This adjustment is needed to

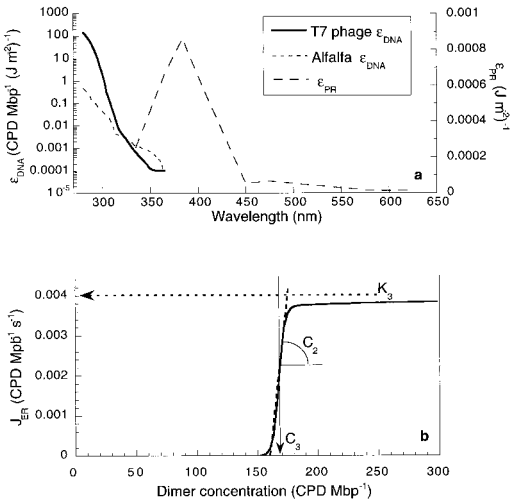

Figure 1. (a) Action spectra for damage and photoreactivation. The action spectrum for pyrimidine dimer induction in T7 bacteriophage is from Emrick and Sutherland (46) and the alfalfa action spectrum is from Quaite *et al.*(48). The photoreactivation action spectrum describes photorepair of dimers in *E. coli*(53). For each spectrum, values were assumed to be zero outside the measured range. (b) Excision repair function. Excision repair is modeled as a combination of a Michaelis–Menten equation and a sigmoidal function. This functional shape has been observed in higher plants (55). Here, the sigmoidal function provides a threshold value (repair occurs above 150 CPD Mbp^{-1}), while the Michaelis–Menten equation leads to a maximal rate at high concentration of dimers. The parameters C_2,C_3 and k_3 are from (Eq. 8).

reconcile experimental values from the literature (mostly on *Escherichia coli*, see above) with data from the field: when a was set to 1.0, all the modeled damage was repaired by photoreactivation, which is inconsistent with observations.

The maximum rate of photoreactivation depends on weighted irradiance:

$$k_2(E) = E^*_{PR}(E) = \int_{335}^{625} E_o(\lambda, t)\cdot\epsilon_{PR}(\lambda)\, d\lambda, \qquad (7)$$

where $\epsilon_{PR}(\lambda)$ is the photoreactivation action spectrum (J m^{-2})$^{-1}$ and E^*_{PR} is the photoreactivation weighted irradiance (s^{-1}). We used the weighting function provided by Sancar *et al.* (k_p in Sancar *et al.* [53] multiplied by 10 to convert from mm^2 ergs^{-1} to [J m^{-2}]$^{-1}$) for photoreactivation in *E. coli* (Fig. 1a) and a maximum rate for k_2 of 0.03 s^{-1} (fig. 3 in Jeffrey *et al.* [11]).

Excision repair. The rate of excision repair of dimers is small relative to that of photoreactivation in bacterioplankton during the day (11); for bacterially mediated virus survival (as measured by plaque assay), photoreactivation is many orders of magnitude greater than excision repair (54). Nonetheless, it is modeled here to give a more complete description of processes affecting net DNA damage, and because it may be important at night when photoreactivation does not occur.

Excision repair in bacterioplankton has not, to our knowledge, been quantified rigorously. Therefore, we modeled the DNA-specific rates of excision repair ($J_{ER}(N)$, CPD Mbp^{-1} s^{-1}) with a heuristic relationship having a functional shape consistent with data obtained by Quaite *et al.* (55, see also Sutherland *et al.* [56]) in higher plants, and with rate constants estimated to fit sparse measurements for bacterioplankton. The relationship is

$$J_{ER}(N) = \frac{k_3\cdot N(t)}{C_1 + N(t)}\cdot\frac{1}{1 + e^{C_2\cdot(C_3 - N(t))}}, \qquad (8)$$

where k_3 is the maximal rate of dimer removal (CPD Mbp^{-1} s^{-1}); C_1 is a constant (CPD Mbp^{-1}) resembling a half-saturation constant in the absence of a threshold; C_2 is a constant (CPD^{-1} Mbp) that governs the ''steepness'' of the ascent; and C_3 is another constant (CPD Mbp^{-1}) that fixes the position of the ascent (Fig. 1b). Equation 8 is largely unconstrained because quantitative experiments for bacterioplankton have not been conducted. The maximum rate, k_3, was set to 0.004 CPD Mbp^{-1} s^{-1}, consistent with measurements on bacterioplankton (see fig. 3 in Jeffrey *et al.* [11]), C_1 was set to 12 CPD Mbp^{-1} and C_2 to 0.4 CPD^{-1} Mbp. This provides a relatively steep threshold and a practically constant repair rate above the threshold. The threshold, C_3, was set following the observation that, before sunrise, in the upper water column of the Gulf of Mexico, there was a background concentration of about 150 CPD Mbp^{-1} (29). Assuming that excision repair had enough time to repair all the damage from the previous day, and that analytical methods were free of an offset, the threshold for repair was fixed at 150 CPD Mbp^{-1}, which leads to a value for C_3 of 168 CPD Mbp^{-1}. With this function, even at maximal rate (a measured parameter [11]), excision repair is small compared to photoreactivation during daylight. Thus, large uncertainties on the function for excision repair only influence the patterns observed at night.

The model is written in MATLAB®, using discrete time steps (5 min) where all parameters remain constant. The total accumulation of CPD is found by integrating numerically the following differential equation with respect to time:

$$\frac{dN}{dt} = J_{dam} - J_{PR} - J_{ER}. \qquad (9)$$

Measurements in the field. Four cruises were carried out to measure the concentration of dimers in oceanic bacterioplankton and small phytoplankton. All data presented in this study, except those from the Gerlache Strait have been previously published (29). Detailed descriptions of data collection, processing and analysis can be found in Jeffrey *et al.* (29) and are summarized here.

In the Gulf of Mexico, on two consecutive days (7 and 8 September 1994), vertical profiles of dimer concentration *in situ* were measured before sunrise and after sunset, by collecting water samples at different depths. The samples were filtered through 0.8 μm filters (Gelman) to exclude phytoplankton and larger particles, and the filtrates were collected on 0.2 μm filters (Gelman), thus allowing smaller particles and viruses to pass through. The concentration of CPD was measured using a radioimmunoassay (polyclonal antibody). Complete details of the technique have been published (57–59); its specificity and sensitivity have been tested extensively and found to be excellent (60–63).

On the same days, DNA dosimeters (64) were deployed: a solution of calf-thymus DNA was dispensed into quartz vials, suspended at different depths, and incubated *in situ* from dawn to dusk. Dosimeters provided a measure of the effective dose, *i.e.* the time-integrated DNA damaging irradiance at depth (65). At noon each day, a vertical profile of downwelling irradiance at 305, 320, 340, 380 nm nominal center wavelengths, and photosynthetically available radiation (PAR) was made using a PUV 500 profiler from Biospherical Inc. (*e.g.* [66]). Water temperature at the surface was 28°C. Both days were sunny; 7 September was windy (around 8 m s^{-1}) while 8 September was calm. Hence, differences in damage profiles should be attributable to mixing (29).

During a cruise in April 1994 in the Gulf of Mexico, a buoy was deployed at 0600 h local time and water samples were collected at the surface ($z < 0.2$ m) within 100 m of the buoy every 3 h for 24 h (29). The samples were processed by the same method as for the vertical profiles. Sea surface temperature was estimated to be 15°C (no direct measurements were made); there was little wind and the sky was clear.

Two cruises were conducted in the Gerlache Strait near Antarctica, in the late spring of 1995 and 1996. Water column conditions are reported in Massana *et al.* (67): sea surface temperatures were −0.65°C in 1995 and −1.5°C in 1996. Sampling, experimentation and analysis were the same as for the Gulf of Mexico in September 1994, with one addition: UV-transparent (UVT) acrylic boxes were filled with 30–50 L of unfiltered seawater and incubated at different depths, to provide an assessment of net damage *in situ* in the absence of vertical mixing.

Implementation of the model. We simulated the three sunny days for which estimates of ozone and wind speed were available: 7 and 8 September 1994 in the Gulf of Mexico and 6 October 1996 in the Gerlache Strait. Mixed layer depths were estimated from density profiles following Jeffrey *et al.* (29) for the Gulf of Mexico and were set to 25 m for the Gerlache Strait (inferred from temperature and salinity profiles in Massana *et al.* [67]). For the irradiance model, we assumed 80% humidity and 23 km visibility. The parameter for air mass type (*AM*, unitless), was set to 1 for all computations, simulating the scattering by open-ocean aerosols (30). Ozone values were obtained from the total ozone mapping spectrometer (TOMS) archives for the corresponding days. Values for K_d were adjusted to match measurements in the UV by varying *DOM* in (Eq. 4), allowing for the interpolation and extrapolation of K_d at wavelengths not measured (68). The model was initialized using profiles of damage measured in the morning, and run from sunrise to sunset. Comparisons between model results and measurements were made using the last time step of the model before sunset. To model DNA damage during *in situ* incubations, vertical mixing was turned off and irradiance was multiplied by the transmittance of UVT acrylic. The quartz vials for DNA dosimeters were assumed to be totally transparent.

Diel changes in the surface water of the Gulf of Mexico were calculated by running the model for the cruise location on 27 April 1994. The modeled DNA damage averaged over the first 30 cm was compared with the measured concentration of dimers at the surface.

A sensitivity analysis was performed to assess sources of variability in DNA damage, using as a reference a simulation for 7 September 1994, in the Gulf of Mexico (Table 2). Under these conditions, z_{Euph} is 109 m. The sensitivity analysis assessed the effect of wind speed (0–30 m s^{-1}), *DOM* (0–0.5 g m^{-3}), mixed layer depth (1–200 m), stratospheric ozone thickness (100–400 Dobson unit [DU]) and the effect of a different action spectrum for damage (the alfalfa seedling action spectrum, [48]). Results of the sensitivity analysis are presented as the mean concentration of damage for three depth ranges: the mixed layer (N_{mix}, CPD Mbp^{-1}), below the mixed layer (N_{submix}, CPD Mbp^{-1}) and the whole euphotic zone (N_{Euph}, CPD Mbp^{-1}).

Table 2. Parameters for the standard run of the sensitivity analysis

Parameter	Value
Location and date	Gulf of Mexico, 7 September
Ozone thickness	291 DU
Wind speed	8 m s^{-1}
Chlorophyll concentration	0.15 mg m^{-3}*
DOM concentration	0 g m^{-3}*
Mixed layer depth	20 m
Initial dimer concentration	150 CPD Mbp^{-1}*

* Constant concentration with depth.

RESULTS AND DISCUSSION

Measurements from the field provided several comparisons with model output. The dosimeter experiments provided measurements of damage in the absence of repair mechanisms and mixing. The incubations in acrylic boxes assessed net bacterial damage excluding mixing but including repair. The water column profiles reflected interactions between repair, damage and mixing processes under different wind regimes.

Testing the model

DNA damage in static extracted DNA. Two simulations were run for 7 September in the Gulf of Mexico (Fig. 2a), one with the T7 bacteriophage damage action spectrum (46) and one with the alfalfa seedling action spectrum (48). The T7 model overestimated CPD more than two-fold at the surface. The discrepancy lies mostly in the absolute value of the damage, as the measurement and the model results have similar rates of decrease with depth (Fig. 2b). This pattern suggests that the shape of the T7 action spectrum is correct but that either the absolute value of the action spectrum or the estimated irradiance at short wavelengths (UVB) is too high. In turn, the slower rate of change with depth for the alfalfa action spectrum (Fig. 2b) is inconsistent with measurements and suggests that its spectral shape is inappropriate, or, less likely, that attenuation coefficients in the UVB may have been underestimated. Only the results for the T7 action spectrum are shown for the simulation of the Gerlache strait (Fig. 2c). Here, the model slightly overestimates CPD at 1 and 2 m. The modeled decrease with depth is similar to what was measured, however, (Fig. 2d), again implying that the T7 action spectrum has the right shape.

DNA damage of natural bacterial assemblages in situ. Water column profiles of CPD *in situ* measure the net result of interactions between damage, repair and mixing processes. Considering the simplicity of the model (compared with *e.g.* [25,26]), simulated profiles of net damage are reassuringly consistent with the measurements (Fig. 3a–c). The effect of wind speed on damage is well reproduced by the model; it explains most of the difference in damage between the calm *vs* windy day (Fig. 3a,b). The changes in the absolute value of the damage are also consistent with measurements for different locations (compare Fig. 3a,b with c).

Model results illustrate the relative importance of repair processes: near the surface (top 5–10 m depending on $K_d(\lambda)$), photoreactivation roughly halves the net damage sustained. In contrast, excision repair is of limited importance during the day (compare ''damage and repair'' to ''damage and photoreactivation'' in Fig. 3). It should be noted that, although the model reproduces the profiles fairly accurately, it overestimates photoreactivation at depth. This may be due to: (1) an overweighting of the weakly attenuated blue light by the photoreactivation action spectrum; (2) an underestimation of the diffuse attenuation coefficient for photoreactive irradiance; or (3) a residual level of measured CPD not associated with functional bacterioplankton.

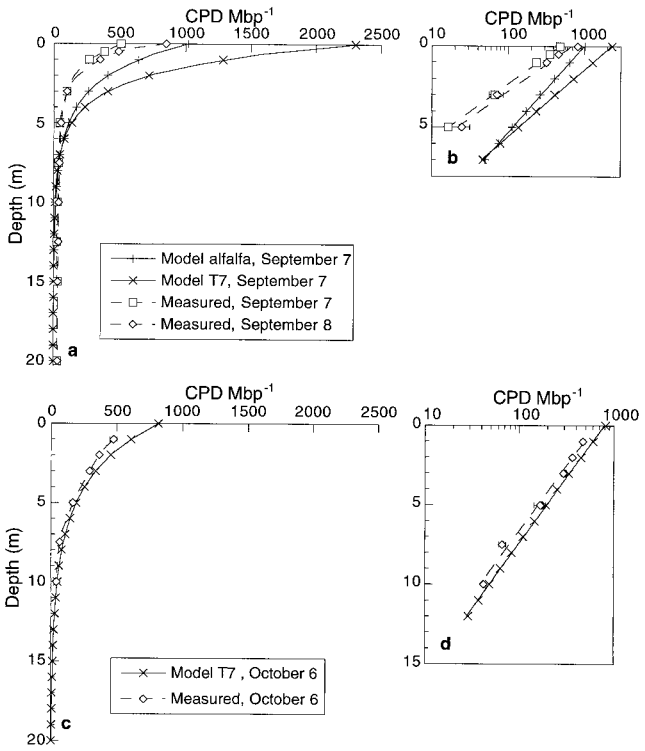

Figure 2. Modeled and measured dosimeter profiles. (a) 7 and 8 September 1994 in the Gulf of Mexico (data are from Jeffrey *et al.* [29]). The model was run twice: once with the action spectrum for the T7 bacteriophage and once with the action spectrum for alfalfa seedlings. Dosimeters were treated in the model as bacterioplankton, but no mixing or repair processes were included. Since modeled damage did not differ appreciably for the 2 days, only the modeled results for 7 September are shown. (b) log-transformed near-surface data from (a). (c) Modeled and measured dosimeter dimer profiles for 6 October 1996 in the Gerlache Strait. Only the model run for the T7 bacteriophage is shown. (d) Log-transformed near-surface data from (c). Log-transformed data strongly suggest that the T7 bacteriophage action spectrum has the right shape for weighting DNA damage in marine bacterioplankton.

Incubation of natural assemblages in situ. Static incubation of natural assemblages *in situ* provides measurements of damage and repair in a nonmixing environment. A comparison of the model without mixing *vs* measurements in the Gerlache Strait (Fig. 4) shows reasonable agreement between 2 and 5 m. Damage at depth is greatly underestimated, however, presumably due to excessive repair in the model. Parameters for repair functions are for bacteria at a warmer temperature; overestimation of repair in the Antarctic is not surprising because enzymatic processes are strongly dependent on temperature (discussed below). The residual damage measured at depth could also come from the presence of dead or inactive cells; it is observed in environmental sam-

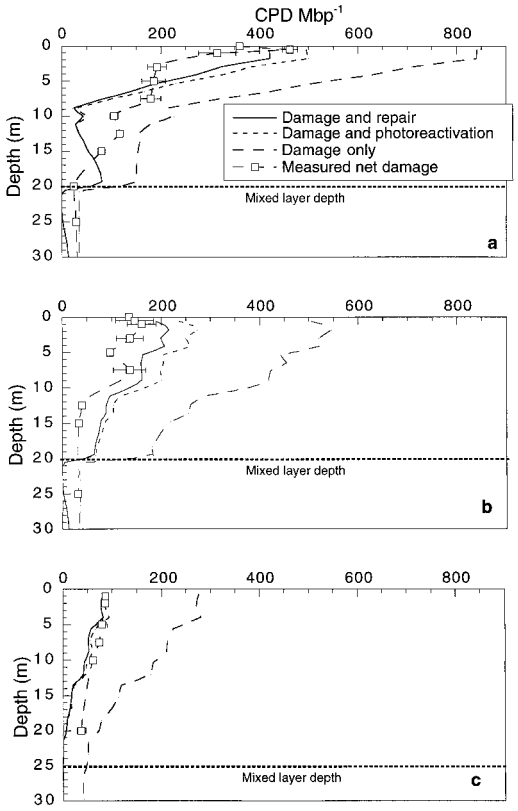

Figure 3. Comparison between modeled and measured dimer profiles for natural assemblages. Modeled profiles are for: damage only; damage plus photoreactivation, which includes only the damage and photoreactivation functions; and damage and repair, which provides the damage and both excision and photoreactivation repair. (a) 8 September 1994 in the Gulf of Mexico. For this run, a mixed layer depth of 20 m was used. The attenuation coefficient was modeled by adding $DOM = 0.3$ g m^{-3} to the clear-water attenuation coefficient (33,34) to fit the measured attenuation (between 305 and 380 nm) coefficient for that day. The ozone concentration was 291 DU as measured by TOMS and the wind speed was set to 2 m s^{-1} as measured on the ship. An initial damage level of 150 CPD Mbp^{-1} was set above the mixed layer and 35 CPD Mbp^{-1} below the mixed layer as measured at 0600 h. The error bars correspond to the standard deviation when triplicate measurements were made at a given depth. Data are from Jeffrey *et al.*(29). (b) 7 September 1994 in the Gulf of Mexico; parameters were the same as for (a) except that wind speed was set to 8 m s^{-1}. Data are from Jeffrey *et al.*(29). (c) 6 October 1996 in the Gerlache Strait. For this run, a mixed layer depth of 25 m was used, the attenuation coefficient was modeled by adding $DOM = 0.12$ g m^{-3} to the clear-water attenuation coefficient (33), the ozone concentration was set to 200 DU and the wind speed was set to 8 m s^{-1}. The initial damage concentration was set to 40 CPD Mbp^{-1} for the entire euphotic zone as measured before sunrise.

ples (Figs. 3 and 4) but not in dosimeter data (Fig. 2). If this is the case, a first-order correction would be to start the simulations with a zero initial damage level and add a background damage level to the final result.

Diel changes of DNA damage in surface waters. Although the absolute value of the damage is different, the model predicts a diel variation of CPD at the surface closely matching observations in the Gulf of Mexico (Fig. 5). Four distinct features are observed in both the measurement and the model. First, each shows a decrease in the concentration of dimers early in the morning. In the model, this is due to excision repair (compare ''damage and photoreactivation'' with ''damage and repair''). Second, the concentration of dimers increases rapidly in the morning. Third, the concentration of damage is maximal around 1500 h. The time lag between maximal irradiance and the maximal concentration of damage is a normal feature of systems where loss is present (here repair and mixing) (69). At this point, the concentration of dimers starts to decrease. In the model, the decrease is due to the transport of less-damaged cells from deeper water through mixing (compare ''damage only'' with ''damage and repair''; both decrease at a similar rate) and through a reduced rate of dimer production. Finally, after sunset (around 1800 h), the decrease continues while only mixing and excision repair occur. In the model, the water column becomes well mixed, a relatively stable concentra-

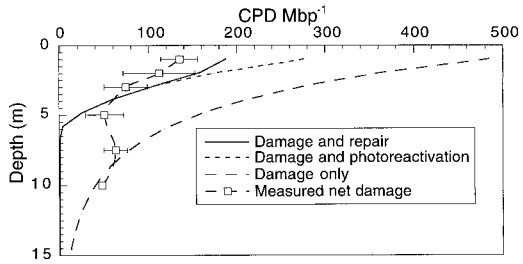

Figure 4. Comparison between measured and modeled DNA damage in UVT acrylic containers suspended in the Gerlache Strait on 6 October 1995. For this run, there was no mixing, the ozone concentration was set to 200 DU and the attenuation coefficient was modeled by adding $DOM = 0.12$ g m^{-3} to the K_d for clear waters (33). The model was initialized with a damage level of 40 CPD Mbp^{-1} to simulate the average dimer concentration measured on that day in the upper 20 m before sunrise. For interpretation of legend see Fig. 3.

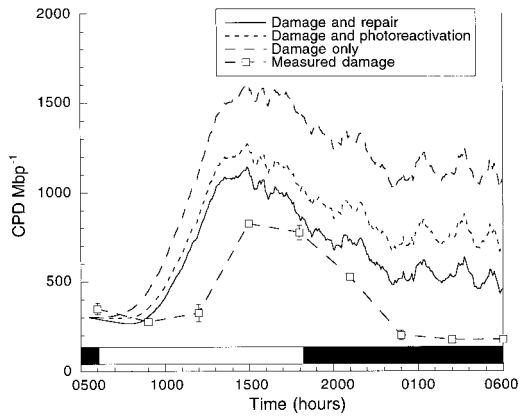

Figure 5. Diel changes in surface dimer concentration for the Gulf of Mexico on 27 April 1994. The irradiance model was run for that day (using the ozone measurement from 27 April 1993), but the attenuation coefficient and wind speed were set to reasonable values as optical and meteorological data were not available: K_d was modeled by adding 0.1 mg m^{-3} of chlorophyll and $DOM = 0.1$ g m^{-3} to the clear water K_d; wind speed was set to 5 m s^{-1} and ozone concentration was set to 290 DU. White bars correspond to the period of daylight. Model parameters were not adjusted to match the absolute values of the measured data. A running average for seven points (35 min) was applied to the model results to provide smoother curves. Data are from Jeffrey *et al.*(29). For interpretation of legend see Fig. 3.

tion is reached and only excision repair reduces the damage level.

The net damage after 24 h is not equal to the damage at the beginning of the experiment, both in the model (though the difference is not large) and in the measurements (see also Lyons *et al.* [59]), showing inverse trends (Fig. 5). This is not surprising since, due to clouds, mixing and other factors, the irradiance regime experienced by the bacteria, hence net damage, varies from day to day in natural systems.

Examining the model

Our idealized representation of UVR-induced damage to DNA and its repair as influenced by mixing in the ocean was developed to provide a quantitative framework for exploring how physical, optical and biological processes interact to determine net damage to DNA. In the following sections, we examine each component of the model.

Mixing. The mixing model (41) improves earlier random walk models that have been used extensively to test the effect of mixing (23,36–40) on different processes by providing a more realistic representation of residence time at depth for plankton. Still, the motions are highly idealized. It has been shown, however, that the choice of mixing model did not significantly change the results in other UV-related work (23). For this reason and because these mixing models have been discussed extensively elsewhere (41, and references therein), the details of the mixing model will not be discussed further.

Irradiance. Comparison of the solar irradiance model with measurements has shown that predictions for the PAR portion of the spectrum are reliable (30), while the extension into the UV range (24) provided good prediction for the days and locations tested (68). The Beer–Lambert law used to propagate the diffuse light field underwater has been tested and measured extensively by numerous authors (*e.g.* [32]) and is adequate for our application.

Damage. The function describing DNA damage is well defined (45) and expected to be correct. However, the use of an action spectrum for a phage instead of one for natural bacterioplankton may lead to discrepancies. First, the relative content of guanine (G) + cytosine (C) *vs* adenine (A) + thymine (T) bases in bacterioplankton DNA may differ from that in the T7 phage (GC content of 50%). This should have consequences for the quantum yield of damage (70) because bacteria with higher GC to AT content have a lower probability of formation of thymine-containing dimers and thus should sustain less CPD for a given UVR dose (54). Phages tend to have a GC content similar to that of their hosts, and measured GC content in marine phages varies from 16 to 70% (54, and references therein). As a result, damage in bacteria could be over- or underestimated by the model. Second, although shielding (71) should not be a concern here due to the small size of the organisms (49), caution is appropriate concerning the absolute values of the action spectra, especially at shorter wavelengths (47,48). Data presented by Joux *et al.* (50) suggest, that an action spectrum for naked DNA is a good approximation for dimer induction in bacterioplankton.

Photoreactivation. The Michaelis–Menten relationship is well established for two-step enzymatic processes, and a light-dependent maximum rate is consistent with photoreactivation (51,53). The rate constants for bacterioplankton are not known, however. Consequently, we applied a scaling factor for photoreactivation to match results from the field. This scaling factor could mask other problems with the formulation, including the use of an inappropriate action spectrum for photoreactivation. Two chromophores associated with photolyase enzymes are known to exist in nature (*e.g.* [72]), and it is not clear which one is utilized by bacterioplankton or if one is common to all species. The action spectrum chosen has a peak efficiency centered around 380 nm typical of the MTHF-type, containing a 5,10-methenyltetrahydrofolate chromophore (*e.g.* [70]). This is consistent with the observation that bacterioplankton seem to have a higher photoreactivation rate when illuminated with UVA than with visible radiation (50). The 8-HDF type of photoreactivation action spectrum (containing 8-hydroxy-5-deazaflavin chromophore), has a peak around 435–445 nm (*e.g.* [73,74]). Using an action spectrum of this type would change the profiles of photoreactivation with depth, but until more work is done the use of an MTHF-type action spectrum seems warranted.

Excision repair. Excision repair is poorly constrained by experimental data. The functional shape (Fig. 1b) is a guess, roughly consistent with data for higher plants (55); the maximum repair rate was measured for bacterioplankton (11), and the three remaining constants (C_1, C_2, C_3 in [Eq. 8]) are based on the best available estimates (see ''Materials and Methods''). Due to the limited importance of excision repair in dimer removal (54), and since its maximum rate, a key parameter, has been measured in bacterioplankton, these limitations are relatively unimportant when assessing the net production of dimers, especially during the day.

Sensitivity analysis

The sensitivity analysis assessed relative influences on DNA damage of varying ozone thickness, CDOM concentration, chlorophyll concentration, wind speed and mixed layer depth (Table 3). In the mixed layer, the most important variations in net damage are caused by changes in ozone thickness and by changes in the depth of the mixed layer. The effects of DOM and chlorophyll concentration are about an order of magnitude lower over the range tested, while wind speed has a minimal effect on the average concentration of damage in the mixed layer. A general understanding of each of these effects can be developed by looking at selected profiles from the sensitivity analysis (Fig. 6).

Ozone thickness. Changes in ozone thickness (Figs. 6a and 7) have the largest effect on DNA damage in the mixed layer: in the upper water column, damage increases as ozone thickness decreases, even more so at lower ozone concentrations. Below the mixed layer (here set at 20 m), the effect of ozone concentration is minimal as most of the DNA-weighted UV radiation is absorbed above this depth. Regardless, the increase in damage in the mixed layer leads to a significant increase in the euphotic zone as a whole (Fig. 7).

Comparison in the mixed layer between the T7 action spectrum and the shielded alfalfa action spectrum (Fig. 7) shows that shielded DNA is less sensitive to decreasing

Table 3. Summary of the sensitivity analysis. For the analysis, one parameter was changed (the varied parameter) over a range of relevant values, while all other parameters in the model were kept constant. Values represent the difference between maximum and minimum average concentration of dimers over the range of the varied parameter. In parentheses are given the highest concentration of dimer modeled and the value of the varied parameter when it occurred (*i.e.* for wind speed in the mixed layer, the highest value observed was 426 CPD Mbp^{-1} at a wind speed of 8 m s^{-1}). Ranges provided here are plausible for natural oceanic conditions. For comparison, the damage for the standard run (Table 2) is equal to 426 CPD Mbp^{-1}. The sign represents the direction of the change (*i.e.* from 8 to 30 m s^{-1}, the damage in the mixed layer *decreased* by 77 CPD Mbp^{-1})

Varied Parameter	Mixed layer $\Delta \bar{N}_{mix}$ (CPD Mbp^{-1})	Euphotic zone $\Delta \bar{N}_{Euph}$ (CPD Mbp^{-1})	Range
Wind speed	−77 (426; 8 m s^{-1})	−10 (159; 8 m s^{-1})	8–30 m s^{-1}*
Mixed layer depth	−1694 (1847; 1 m)	0 (160; 20 m)	1–100 m*
Ozone thickness	−5235 (5621; 100 DU)	−965 (1118; 100 DU)	100–300 DU
	−1757 (2143; 150 DU)	−325 (477; 150 DU)	150–300 DU
DOM	−299 (426; 0 g m^{-3})	−22 (160; 0 g m^{-3})	0–0.5 g m^{-3}*†
Chlorophyll concentration (and covarying matter)	−345 (529; 0 mg m^{-3})	46 (186; 0 mg m^{-3})	0–2 mg m^{-3}*†

* The range corresponds to the range for which the maximum variation in modeled damage occurred in the mixed layer.
† Changing the concentration also affected the euphotic zone depth.

ozone thickness in absolute and in relative terms (see [47,48]); the slope of the action spectrum and its absolute value are much lower at short UVB wavelengths. The alfalfa action spectrum, which is consistent with screening of UVB by cellular compounds (48) and perhaps with other secondary mechanisms (75), is not likely to be representative of bacterioplankton.

The inset graph in Fig. 7 shows the same data (except for the alfalfa curve) as in the main figure, but plotted relative to 300 DU. This presentation is commonly used to illustrate amplification factors (discussed below). Clearly, the two graphs may lead to a different interpretation if care is not taken.

Amplification factors are used to relate a given effect to changes in ozone thickness. Here, we use the power law adopted by Booth and Madronich (76) for the radiation amplification factor (RAF, unitless), applying it to the total amplification factor (TAF, unitless) (1). The RAF relates the increase in a given measure of irradiance (usually weighted irradiance) to a decrease in ozone thickness, while TAF relates a biological effect to ozone thickness (1). For net damage to DNA in a stratum of the water column as a function of ozone thickness:

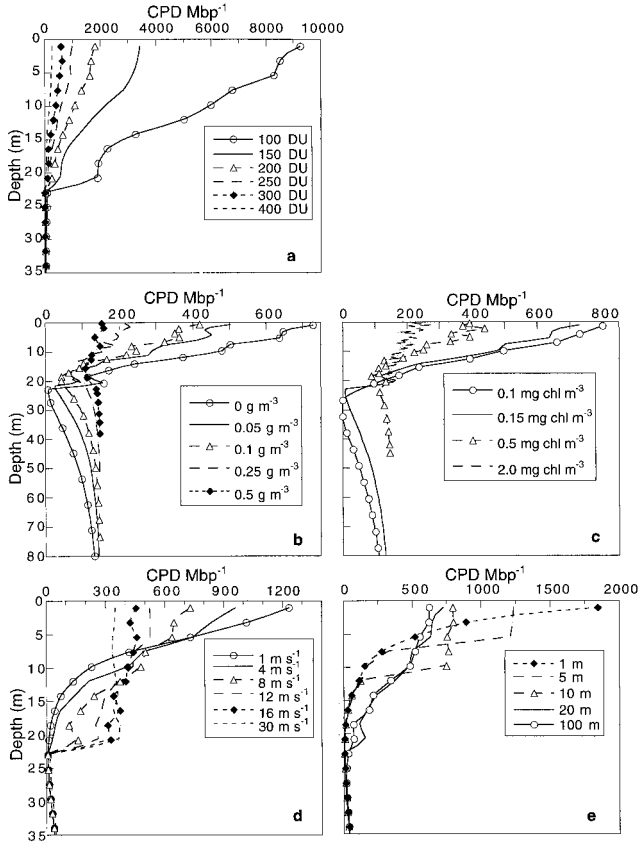

Figure 6. Net DNA damage in vertical profiles from selected sensitivity analysis results: (a) Ozone, (b) DOM concentration, (c) chlorophyll concentration, (d) wind speed and (e) mixed layer depth. Parameters for the standard run of the sensitivity analysis are provided in Table 2.

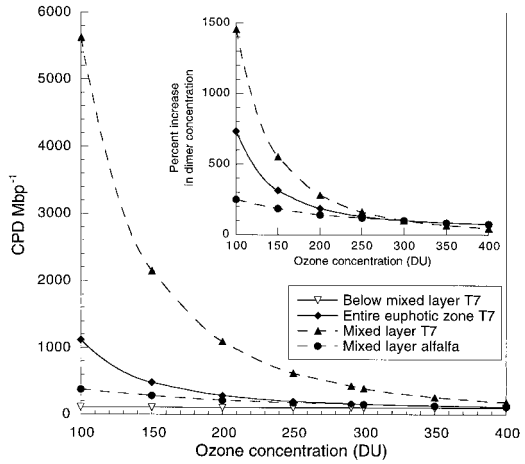

Figure 7. Sensitivity analysis for the effect of ozone thickness and damage action spectra on DNA damage. The inset graph shows the results for the mixed layer expressed in percent change relative to 300 DU. Parameters for the standard run of the sensitivity analysis are provided in Table 2.

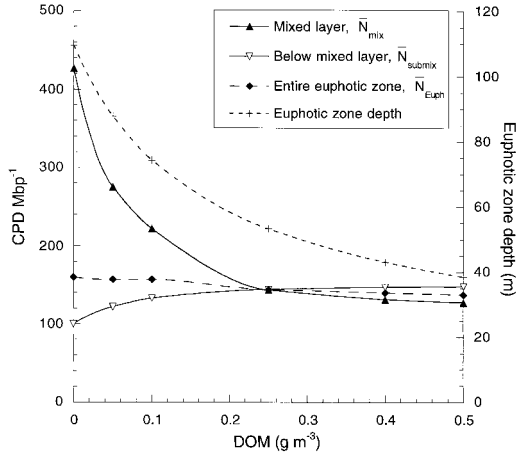

Figure 8. Sensitivity analysis for the effect of DOM on DNA damage. The change in the euphotic zone depth is also shown. Parameters for the standard run of the sensitivity analysis are provided in Table 2.

$$\frac{N_2}{N_1} = \left(\frac{\omega_2}{\omega_1}\right)^{-TAF}, \qquad (10)$$

where ω_i is ozone thickness and N_i is average CPD concentration in the stratum at the end of the day for each of two ozone thicknesses *i*. When more than two measurements are used, TAF is found by fitting a linear function to log-transformed data. Using the T7 bacteriophage action spectrum, we obtained a $TAF_{Euph} = 1.7$ for the whole euphotic zone (109 m) and $TAF_{mix} = 2.5$ for a mixed layer of 20 m. For comparison, RAF obtained for generalized DNA damage (77) at the surface varies from 2.1 to 2.2 depending on time of year (78). Our estimate of TAF are, to the best of our knowledge, the only amplification factors for net damage to DNA that have been calculated for the water column. Usually, RAF is derived for weighted irradiance at the surface (78).

Effect of CDOM and chlorophyll concentration. CDOM and chlorophyll concentration (including covarying matter) have similar effects on net damage to DNA (Fig. 6b,c and Fig. 8 for DOM). First, an increase in concentration decreases the depth of the euphotic zone, particularly in the case of chlorophyll. Second, penetration of irradiance at shorter, more damaging wavelengths is reduced relative to that of irradiance at longer, photoreactivating wavelengths (79); this is especially important in the case of CDOM. In the mixed layer, an increase in chlorophyll or CDOM concentration leads to a decrease in damage, as more of the damaging radiation is absorbed by these substances. Since little damage occurs below the mixed layer, and the model is initialized with a nonzero concentration of damage, the effect at depth is due to influences on repair. At low concentrations of CDOM or chlorophyll more photoreactivating light penetrates and photoreactivation can repair damage efficiently below the mixed layer. As the concentration of chlorophyll or CDOM increases in the mixed layer, less photoreactivating light reaches below the mixed layer, and less photorepair occurs. This leads to a greater concentration of damage at depth. In the limiting case where no photoreactivating irradiance penetrates below the mixed layer, the initial concentration of 150 CPD Mbp^{-1} will be maintained (Fig. 8). Although this shows the expected trends, this situation is unrealistic as it is hard to imagine, under these conditions, a process by which so much damage could be present below the mixed layer. To summarize, as the concentration of CDOM increases, the ratio of E^*_{DNA}/E^*_{PR} decreases and this decrease is greater at depth. The same applies to increases in chlorophyll concentration, but the effect is due to matter that covaries with chlorophyll, not the algal pigment.

The effect of different CDOM concentrations on primary productivity as influenced by UVR has been modeled without considering mixing (79). The results were similar to what is observed in our model for DNA damage. By absorbing photoinhibiting irradiance, an increase in CDOM would enhance productivity in surface waters, but decrease productivity in deeper waters by absorbing PAR. The two effects counteract one another, and the net result of changes in CDOM concentration was small for depth-integrated primary production.

Wind speed. Wind is the sole source of mixing in the model. The higher the wind speed, the shorter the residence time of the particles at a given depth. The effect of wind speed on the net damage in the mixed layer is small (Table 3); under the conditions tested, neither damage nor photoreactivation for the bacterial populations as a whole are strongly influenced by mixing rate. At higher wind speeds, transmission of photoreactivating radiation through the surface decreases slightly, so there is a corresponding decrease in the mixed layer damage.

Although wind mixing has a small effect on average damage in a mixed layer of fixed depth, changing the wind speed strongly modifies the distribution of damage in the mixed layer (Fig. 6d). As wind speed increases, the near-surface damage is mixed downward and the damage tends toward a uniform distribution with depth. This difference will lead to important ecological consequences (68) if the relationship between an ecologically relevant parameter (*e.g.* survival, productivity or viral infectivity) and CPD concentration is nonlinear (*e.g.* [50,80]).

Mixed layer depth. The depth of the mixed layer has important consequences for the concentration of DNA damage within it (Table 3, Fig. 6e). As the mixed layer shoals, particles are ''cycled'' more rapidly within an environment where the ratio of damage to photoreactivation is increasing, so damage levels increase (see discussion in Pakulski *et al.* [16]). However, this effect is not seen over the whole euphotic zone as the average damage level in the euphotic zone is nearly constant over a range of mixed layer depth of 1–100 m.

Further considerations

Other ecological processes. Although a biological model is proposed here, it does not include any ecological processes such as grazing, lysis or multiplication of bacterial cells. With typical rates of bacterial growth of 1–2 day^{-1} in the natural environment, these processes may affect the results (discussed in Jeffrey *et al.* [29]): the method for measuring the concentration of dimers does not detect DNA from lysed cells (as it will pass through the filter), and it will be affected by ''the dilution'' of damage by reproduction. The model

also assumes that all cells are active (in this context, signifies that they can repair damage) and that the rate of excision repair is constant throughout the day.

Other effects of CDOM. The effect of CDOM on bacterial ecology cannot be assessed solely by considering its photoprotective capability (81). In fact, photodegradation of CDOM, which can lead to increased or decreased bioavailability of substrate for bacterial growth (seemingly depending on its source), may overshadow the importance of photoprotection by increasing or inhibiting bacterial activity (19,20,81–83). Consequently, interactions of UVR and CDOM are complex. Photodegradation of CDOM can alter bacterial production indirectly, but photodegradation also leads to bleaching (*e.g.* [84]), hence increased susceptibility of bacteria to direct DNA damage. The different time scales of these processes confuses things even more. Net damage to DNA cycles on a daily basis (85); photochemical processes affecting CDOM also occur on a daily basis, but bleaching of CDOM is slow. Significant bleaching seems to occur on time scales of months in the mixed layer of the ocean (as discussed by Nelson *et al.* [86]).

Temperature. The effect of temperature is not addressed in the model. Only the two enzymatic processes, excision repair and photoreactivation, should be strongly influenced by temperature. Excision repair is slow, and any changes induced by temperature should not have a significant effect on the repair of dimers during the day. In contrast, the effect of temperature on photoreactivation could be important. The Q_{10} for photoreactivation is of the order of 1–3 between 15 and 37°C, and slightly higher (~5) between 3 and 15°C (87). This temperature dependence is due to the first step (dark-step) of photoreactivation (70). Hence, if the model remained the same except for the temperature dependence, the repair rates in the Gerlache Strait (Figs. 3c and 4) would have been about 10 times slower. This said, organisms living in this environment have adapted to cold conditions and may have compensated for lower enzyme-specific repair rates by other mechanisms for countering the effects of UVR. It is not clear which strategies are used, but the same UV-tolerance mechanisms have been found in Antarctic organisms as for those from lower latitudes (3,88).

Reciprocity. Unlike current models of photoinhibition of photosynthesis (*e.g.* [24,89]), this model treats repair and damage mechanisms separately, thereby obviating the reciprocity issue (45,90) by dealing with it explicitly. That is, damage depends only on dose (*i.e.* shows reciprocity) if only damage occurs, but net damage will show some dose-rate dependence if repair also occurs.

Survival and inhibition of activity. Ultimately, we wish to describe the survival of bacteria or inhibition of their productivity due to, or correlated with, the concentration of dimers. Such relationships are suggested by contextual evidence (*e.g.* [28,29,91]) whereby activity is reduced when DNA damage occurs, and activity is regained when damage to DNA is allowed to repair (92). However, we are aware of no research describing direct relationships between productivity and DNA damage in bacterioplankton. The relationship between survival and dimer concentration for laboratory isolates of bacterioplankton has been studied by Joux *et al.* (50); it seems highly variable between species. In this preliminary study, we have shown that it is possible to predict the amount of DNA damage induced by UV radiation under a variety of meteorological and oceanographic conditions. If a good relationship exists between DNA damage and activity of bacterial populations, then activity levels can be predicted. Alternatively, using spectral weighting functions for the inhibition of activity in bacteria (93), it is possible to recast the model in terms of metabolic activity and create a numerical simulation that is similar to those of photoinhibition of photosynthesis (45,94).

Extension to phytoplankton. Modeling DNA damage in phytoplankton (3,88,95) is not, in principle, different from modeling damage in bacteria, except perhaps for consideration of screening by cellular compounds. However, estimating effects of UVR on growth rates of phytoplankton is not as straightforward as for bacterioplankton. In phytoplankton, two UV-mediated factors will reduce growth rate: DNA damage and photoinhibition of photosynthesis. Cells with damaged DNA can continue to photosynthesize, but they cannot divide as damage blocks the replication of the DNA (3,96,97). Inhibition of photosynthesis reduces growth rate by limiting the energy and building material necessary to produce new cells. Nevertheless, if DNA damage is a good indicator of growth rate reduction (referring to a change in cell number) in phytoplankton (as seems to be suggested by recent studies [95,96]), the model presented here could also be used to estimate growth inhibition by UV in phytoplankton in the upper water column. Results could be compared directly to estimates of inhibition of photosynthesis (23,98).

Model limitation and future work. We have shown that, although some parameters are not quantified precisely, the model can provide good estimates of DNA damage in nature. Still, the model requires improvements. First, a photoreactivation action spectrum should be determined for bacterioplankton, and the two rate constants of the Michaelis–Menten equation should be measured. Second, a better constrained relationship for excision repair is needed. Third, although it is likely that the action spectrum for DNA damage used in this study is well suited for bacteria, it would be preferable to measure an action spectrum for DNA damage in bacterioplankton. With these new measurements, stricter constraints will be put on the model and better predictions will be possible.

CONCLUSION

Our model can provide realistic estimates of DNA damage in small-sized plankton. The sensitivity analysis has shown that ozone thickness and the depth of the mixed layer play crucial roles in determining net DNA damage in the mixed layer, but that the dynamics are much different when the whole euphotic zone is considered. The effect of mixing rate on the average damage in the mixed layer is small, but the distribution of damage changes and this may lead to important biological effects. The model allows the determination of TAF for the mixed layer and the whole euphotic zone; these are different from conventional RAF for DNA damage calculated for the surface. The shortcomings of the model clearly expose some of the unanswered questions about net DNA damage and its relationship with bacterial activity in oceanic systems. We have proposed measurements that

would improve the model accuracy and the understanding of UV effects on bacterioplankton. If these measurements were made, not only for bacterioplankton, but also for phytoplankton, the model could provide a quantitative method for determining which has the greater influence on planktonic dynamics: DNA damage or photoinhibition of photosynthesis.

Acknowledgments—We thank Ralph E. Smith, Bill Miller, Catherine Brown, Sophie Johannessen, Marlon Lewis and Geoff MacIntyre, who commented on earlier versions of this work. Jim Kerr and John C. Sutherland provided data for the model, and two anonymous reviewers provided stimulating suggestions. Supported by NSERC, ONR and NSF Polar Programs. This is CEOTR publication #20.

REFERENCES

1. Smith, R. C. and J. J. Cullen (1995) Effects of UV radiation on phytoplankton. *Rev. Geophys.* **33** (Suppl.), 1211–1223.
2. Häder, D.-P., H. D. Kumar, R. C. Smith and R. C. Worrest (1998) Effects on aquatic ecosystems. In *Environmental Effects of Ozone Depletion: 1998 Assessment* (Edited by UNEP), pp. 86–112. UNEP, Nairobi.
3. Karentz, D., J. E. Cleaver and D. L. Mitchell (1991) Cell survival characteristics and molecular responses of Antarctic phytoplankton to ultraviolet-B radiation. *J. Phycol.* **27**, 326–341.
4. Boelen, P., I. Obernosterer, A. A. Vink and A. G. J. Buma (1999) Attenuation of biologically effective UV radiation in tropical Atlantic waters measured with a biochemical DNA dosimeter. *Photochem. Photobiol.* **69**, 34–40.
5. Neale, P. J. (1987) Algal photoinhibition and photosynthesis in the aquatic environment. In *Photoinhibition* (Edited by D. J. Kyle, C. B. Osmond and C. J. Arntzen), pp. 39–65. Elsevier, Amsterdam.
6. Zepp, R. G., T. V. Callaghan and D. J. Erickson (1995) Effects of increased ultraviolet radiation on biogeochemical cycles. *Ambio* **24**, 181–187.
7. Vincent, W. F. and S. Roy (1993) Solar ultraviolet-B radiation and aquatic primary production: damage, protection and recovery. *Environ. Rev.* **1**, 1–12.
8. Franklin, L. A. and R. M. Forster (1997) The changing irradiance environment: consequences for marine macrophyte physiology, productivity and ecology. *Eur. J. Phycol.* **32**, 207–232.
9. Bothwell, M. L., D. M. J. Sherbot and C. M. Pollock (1994) Ecosystem response to solar ultraviolet-B radiation: influence of trophic-level interactions. *Science* **265**, 97–100.
10. Suttle, C. A. and F. Chen (1992) Mechanisms and rates of decay of marine viruses in seawater. *Appl. Environ. Microbiol.* **58**, 3721–3729.
11. Jeffrey, W. H., J. P. Kase and S. W. Wilhelm (2000) Ultraviolet radiation effects on bacterioplankton and viruses in marine ecosystems. In *Effects of UV Radiation on Marine Ecosystems* (Edited by S. J. de Mora, S. Demers and M. Vernet), pp. 206–236. Cambridge University Press, Cambridge.
12. Karl, D., R. Letelier, L. Tupas, J. Dore, J. Christian and D. Hebel (1997) The role of nitrogen fixation in the biogeochemical cycling in the Subtropical North Pacific Ocean. *Nature* **388**, 533–538.
13. Fenchel, T., G. M. King and T. H. Blackburn (1998) *Bacterial Biogeochemistry: The Ecophysiology of Mineral Cycling.* Academic Press, San Diego.
14. Jeffrey, W. H., P. Aas, M. M. Lyons, R. B. Coffin, R. J. Pledger and D. L. Mitchell (1996) Ambient solar radiation-induced photodamage in marine bacterioplankton. *Photochem. Photobiol.* **64**, 419–427.
15. Cho, B. C. and F. Azam (1990) Biogeochemical significance of bacterial biomass in the ocean's euphotic zone. *Mar. Ecol. Prog. Ser.* **63**, 253–259.
16. Pakulski, J. D., P. Aas, W. Jeffrey, M. Lyons, L. Von Waasenbergen, D. Mitchell and R. Coffin (1998) Influence of light on bacterioplankton production and respiration in a subtropical coral reef. *Aquat. Microb. Ecol.* **14**, 137–148.
17. Herndl, G. J. (1997) Role of ultraviolet radiation on bacterioplankton activity. In *The Effect of Ozone Depletion on Aquatic Ecosystems* (Edited by D.-P. Häder), pp. 143–154. Landes, Austin.
18. Gieskes, W. W. C. and A. G. J. Buma (1997) UV damage to plant life in a photobiologically dynamic environment: the case of marine phytoplankton. *Plant Ecol.* **128**, 16–25.
19. Miller, W. M. and M. A. Moran (1997) Interaction of photochemical and microbial processes in the degradation of refractory dissolved organic matter from a coastal marine environment. *Limnol. Oceanogr.* **42**, 1317–1324.
20. Benner, R. and B. Biddanda (1998) Photochemical transformations of surface and deep marine dissolved organic matter: effects on bacterial growth. *Limnol. Oceanogr.* **43**, 1373–1378.
21. Pausz, C. and G. J. Herndl (1999) Role of ultraviolet radiation on phytoplankton extracellular release and its subsequent utilization by marine bacterioplankton. *Aquat. Microb. Ecol.* **18**, 85–93.
22. Murray, A. G. and G. A. Jackson (1993) Viral dynamics II: a model of the interaction of ultraviolet light and mixing processes on virus survival in seawater. *Mar. Ecol. Prog. Ser.* **102**, 105–114.
23. Neale, P. J., R. F. Davis and J. J. Cullen (1998) Interactive effects of ozone depletion and vertical mixing on photosynthesis of Antarctic phytoplankton. *Nature* **392**, 585–589.
24. Arrigo, K. R. (1994) Impact of ozone depletion on phytoplankton growth in the Southern Ocean: large-scale spatial and temporal variability. *Mar. Ecol. Prog. Ser.* **114**, 1–12.
25. Sikorski, R. J. and R. G. Zika (1993) Modeling mixed-layer photochemistry of H_2O_2: physical and chemical modeling of distribution. *J. Geophys. Res.* **98**, 2329–2340.
26. Sikorski, R. J. and R. G. Zika (1993) Modeling mixed-layer photochemistry of H_2O_2: optical and chemical modeling of production. *J. Geophys. Res.* **98**, 2315–2328.
27. Herndl, G. J., G. Müller-Niklas and J. Frick (1993) Major role of ultraviolet-B in controlling bacterioplankton growth in the surface layer of the ocean. *Nature* **361**, 717–719.
28. Visser, P. M., E. Snelder, A. J. Kop, P. Boelen, A. G. J. Buma and F. C. van Duyl (1999) Effects of UV radiation on DNA photodamage and production in bacterioplankton in the coastal Caribbean Sea. *Aquat. Microb. Ecol.* **20**, 49–58.
29. Jeffrey, W. H., R. J. Pledger, P. Aas, S. Hager, R. B. Coffin, R. Von Haven and D. L. Mitchell (1996) Diel and depth profiles of DNA photodamage in bacterioplankton exposed to ambient solar ultraviolet radiation. *Mar. Ecol. Prog. Ser.* **137**, 283–291.
30. Gregg, W. W. and K. L. Carder (1990) A simple spectral solar irradiance model for cloudless maritime atmosphere. *Limnol. Oceanogr.* **35**, 1657–1675.
31. Prieur, L. and S. Sathyendranath (1981) An optical classification of coastal and oceanic waters based on the specific spectral absorption curves of phytoplankton pigments, dissolved organic matter, and other particulate materials. *Limnol. Oceanogr.* **26**, 671–689.
32. Gordon, H. R. (1989) Can the Lambert–Beer law be applied to the diffuse attenuation coefficient of ocean water? *Limnol. Oceanogr.* **34**, 1389–1409.
33. Baker, K. S. and R. C. Smith (1982) Bio-optical classification and model of natural waters. *Limnol. Oceanogr.* **27**, 500–509.
34. Smith, R. C. and K. S. Baker (1981) Optical properties of the clearest natural waters (200–800 nm). *Appl. Opt.* **20**, 177–184.
35. Morel, A. (1978) Available, usable, and stored radiant energy in relation to marine photosynthesis. *Deep-Sea Res.* **25**, 673–687.
36. Woods, J. D. and R. Onken (1982) Diurnal variation and primary production in the ocean—preliminary results of a lagrangian ensemble model. *J. Plankton Res.* **4**, 735–756.
37. Falkowski, P. G. and C. D. Wirick (1981) A simulation model of the effects of vertical mixing on primary productivity. *Mar. Biol.* **65**, 69–75.
38. Yamazaki, H. and D. Kamykowski (1991) The vertical trajectories of motile phytoplankton in a wind-mixed water column. *Deep-Sea Res.* **38**, 219–241.
39. Franks, P. J. S. and J. Marra (1994) A simple new formulation for phytoplankton photoresponse and an application in a wind-driven mixed-layer model. *Mar. Ecol. Prog. Ser.* **111**, 145–153.

40. Lizon, F., L. Seuront and Y. Lagadeuc (1998) Photoadaptation and primary production study in tidally mixed coastal waters using a lagrangian model. *Mar. Ecol. Prog. Ser.* **169**, 43–54.
41. Visser, A. W. (1997) Using random walk models to simulate the vertical distribution of particles in a turbulent water column. *Mar. Ecol. Prog. Ser.* **158**, 275–281.
42. Yamazaki, H. and D. Kamykowski (1994) Reply to Greg Holloway. *Deep-Sea Res. I* **41**, 961–963.
43. Holloway, G. (1994) Comment: on modelling vertical trajectories of phytoplankton in a mixed layer. *Deep-Sea Res. I* **41**, 957–959.
44. Large, W. G., J. C. McWilliams and S. C. Doney (1994) Oceanic vertical mixing: a review and a model with a nonlocal boundary layer Parameterization. *Rev. Geophys.* **32**, 363–403.
45. Cullen, J. J. and P. J. Neale (1997) Biological weighting functions for describing the effects of ultraviolet radiation on aquatic systems. In *The Effects of Ozone Depletion on Aquatic Ecosystems* (Edited by D.-P. Häder), pp. 97–118. Landes, Austin.
46. Emrick, A. and J. C. Sutherland (1989) Action spectra for formation of pyrimidine dimers in T7 DNA: 180 to 365 nm. *Photochem. Photobiol.* **49**, 35S.
47. Sutherland, B. M. (1995) Action spectroscopy in complex organisms: potentials and pitfalls in predicting the impact of increased environmental UVB. *J. Photochem. Photobiol. B: Biol.* **31**, 29–34.
48. Quaite, F. E., B. M. Sutherland and J. C. Sutherland (1992) Action spectra for DNA damage in alfalfa lowers predicted impact of ozone depletion. *Nature* **358**, 576–578.
49. Garcia-Pichel, F. (1994) A model for the internal self-shading in planktonic organisms and its implications for the usefulness of ultraviolet sunscreens. *Limnol. Oceanogr.* **39**, 1704–1717.
50. Joux, F., W. H. Jeffrey, P. Lebaron and D. L. Mitchell (1999) Marine bacterial isolates display diverse responses to UV-B radiation. *Appl. Environ. Microbiol.* **65**, 3820–3827.
51. Harm, W., C. S. Rupert and H. Harm (1971) The study of photoenzymatic repair of UV lesions in DNA by flash photolysis. In *Photophysiology*, Vol. 6 (Edited by A. C. Giese), pp. 279–324. Academic Press, New York.
52. Blattner, F. R., G. Plunkett, III, C. A. Bloch, N. T. Perna, V. Burland, M. Riley, J. Collado-Vides, J. D. Glasner, C. K. Rode, G. F. Mayhew, J. Gregor, N. W. Davis, H. A. Kirkpatrick, M. A. Goeden, D. J. Rose, B. Mau and Y. Shao (1997) The complete genome of *Escherichia coli* K-12. *Science* **277**, 1453–1474.
53. Sancar, G. B., M. S. Jorns, G. Paynet, D. J. Fluke, C. S. Rupert and A. Sancar (1987) Action mechanism of *Escherichia coli* DNA photolyase. *J. Biol. Chem.* **262**, 492–498.
54. Kellogg, C. A. (1998) Genetic Diversity and DNA Repair of Marine Vibriophage. Ph.D. thesis, University of South Florida, St. Petersburg.
55. Quaite, F. E., S. Takayanagi, J. Ruffini, J. C. Sutherland and B. M. Sutherland (1994) DNA damage levels determine cyclobutyl pyrimidine dimer repair mechanisms in alfalfa seedlings. *Plant Cell* **6**, 1635–1641.
56. Sutherland, B. M., S. Takayanagi, J. H. Sullivan and J. C. Sutherland (1996) Plant responses to changing environmental stress: cyclobutyl pyrimidine dimer repair in soybean leaves. *Photochem. Photobiol.* **64**, 464–468.
57. Mitchell, D. L. (1999) Quantification of photoproducts in mammalian cell DNA using radioimmunoassay. *Methods Mol. Biol.* **113**, 165–173.
58. Mitchell, D. L. (1996) Radioimmunoassay of DNA damaged by ultraviolet light. In *Technologies for DNA Damage and Mutations* (Edited by G. Pfeiffer), Plenum, New York.
59. Lyons, M. M., P. Aas, J. D. Pakulski, L. Van-Waasbergen, R. V. Miller, D. L. Mitchell and W. H. Jeffrey (1998) DNA damage induced by ultraviolet radiation in coral-reef microbial communities. *Mar. Biol.* **130**, 537–543.
60. Mitchell, D. L., J. M. Clarkson, C. C.-k. Chao and B. S. Rosenstein (1986) Repair of cyclobutane dimers and (6-4) photoproducts in ICR 2A frog cells. *Photochem. Photobiol.* **43**, 595–597.
61. Tang, M.-S., J. Hrncir, D. L. Mitchell, J. Ross and J. Clarkson (1986) The relative cytotoxicity and mutagenicity of cyclobutane pyrimidine dimers and (6-4) photoproducts in *Escherichia coli* cells. *Mutat. Res.* **161**, 9–17.
62. Mitchell, D. L., J. E. Vaughn and R. S. Nairn (1989) Inhibition of transient gene expression in Chinese hamster ovary cells by cyclobutane dimers and (6-4) photoproducts in transfected UV-irradiated plasmid DNA. *Plasmid* **21**, 21–30.
63. Gosh, R., D. Johnston and D. L. Mitchell (1995) Generation of oligonucleotides containing site-specific cyclobutane pyrimidine dimers and pyrimidine (6-4) pyrimidinone photoproducts by immunoprecipitation. *Nucleic-Acids Res.* **23**, 4934–4937.
64. Regan, J. D., W. L. Carrier, H. Gucinski, B. L. Olla, H. Yoshida, R. K. Fujimura and R. I. Wicklund (1992) DNA as a solar dosimeter in the ocean. *Photochem. Photobiol.* **56**, 35–42.
65. Horneck, G. (1997) Biological UV dosimetry. In *The Effects of Ozone Depletion on Aquatic Ecosystems* (Edited by D.-P. Häder), pp. 119–142. Landes, Austin.
66. Kirk, J. T. O., B. R. Hargreaves, D. P. Morris, R. B. Coffin, B. David, D. Frederickson, D. Karentz, D. R. S. Lean, M. P. Lesser, S. Madronich, J. H. Morrow, N. B. Nelson and N. M. Scully (1994) Measurement of UV-B in two freshwater lakes: an instrument intercomparison. *Arch. Hydrobiol. Beih Ergebn. Limnol.* **43**, 71–99.
67. Massana, R., L. T. Taylor, A. E. Murray, K. Y. Wu, W. H. Jeffrey and E. F. DeLong (1998) Vertical distribution and temporal variation of marine planktonic archea in the Gerlache Strait, Antarctica, during early spring. *Limnol. Oceanogr.* **43**, 607–617.
68. Huot, Y. (1999) Damage to DNA in bacterioplankton: a model of damage by ultraviolet radiation and its repair as influenced by vertical mixing. Masters thesis, Dalhousie University, Halifax.
69. Doney, S. C., R. G. Najjar and S. Stewart (1995) Photochemistry, mixing and diurnal cycles in the upper ocean. *J. Mar. Res.* **53**, 341–369.
70. Harm, W. (1980) *Biological effects of ultraviolet radiation.* Cambridge University Press, New York.
71. Sutherland, B. M. (1997) UV effects in ''the real world'': problems of UV dosimetry in complex organisms. *J. Photochem. Photobiol. B: Biol.* **40**, 8–13.
72. Kim, S.-T. and A. Sancar (1993) Photochemistry, photophysics, and mechanism of pyrimidine dimer repair by DNA photolyase. *Photochem. Photobiol.* **57**, 895–904.
73. Jagger, J., H. Takebe and J. M. Snow (1970) Photoreactivation of killing in *Streptomyces*: action spectra and kinetic studies. *Photochem. Photobiol.* **12**, 185–196.
74. Eker, A. P. M., P. Kooiman, J. K. C. Hessels and A. Yasui (1990) DNA photoreactivating enzyme from the cyanobacterium *Anacystis nidulans. J. Biol. Chem.* **265**, 8009–8015.
75. Hoque, E. and G. Remus (1999) Natural UV-screening mechanisms of Norway spruce (*Picea abies* [L.] Karst.) needles. *Photochem. Photobiol.* **69**, 177–192.
76. Booth, C. R. and S. Madronich (1994) Radiation amplification factors: improved formulation accounts for large increases in ultraviolet radiation associated with Antarctic ozone depletion. In *Ultraviolet Radiation in Antarctica: Measurements and Biological Effects*, Vol. 62 (Edited by C. S. Weiler and P. A. Penhale), pp. 39–42. American Geophysical Union, Washington.
77. Setlow, R. B. (1974) The wavelengths in sunlight effective in producing skin cancer: a theoretical analysis. *Proc. Natl. Acad. Sci. USA* **71**, 3363–3366.
78. Madronich, S., R. L. McKenzie, L. O. Björn and M. M. Caldwell (1998) Changes in biologically active ultraviolet radiation reaching the earth's surface. In *Environmental Effects of Ozone Depletion: 1998 cassessment* (Edited by UNEP), pp. 1–27. UNEP, Nairobi.
79. Arrigo, K. R. and C. W. Brown (1996) Impact of chromophoric dissolved organic matter on UV inhibition of primary productivity in the sea. *Mar. Ecol. Prog. Ser.* **140**, 207–216.
80. Wilhelm, S. W., M. G. Weinbauer, C. A. Suttle, R. J. Pledger and D. L. Mitchell (1998) Measurements of DNA damage and photoreactivation imply that most viruses in marine surface waters are infective. *Aquat. Microb. Ecol.* **14**, 215–222.
81. Herndl, G. J., A. Brugger, S. Hager, E. Kaiser, I. Obernosterer,

B. Reitner and D. Slezak (1997) Role of ultraviolet-B radiation on bacterioplankton and the availability of dissolved organic matter. *Plant Ecol.* **128**, 42–51.
82. Lindell, M. J., H. W. Granéli and L. J. Tranvik (1995) Enhanced bacterial growth in response to photochemical transformation of dissolved organic matter. *Limnol. Oceanogr.* **40**, 195–199.
83. Lindell, M. J., H. W. Granéli and L. J. Tranvik (1996) Effects of sunlight on bacterial growth in lakes of different humic content. *Aquat. Microb. Ecol.* **11**, 135–141.
84. Vodacek, A., N. V. Blough, M. D. Degrandpre, E. T. Peltzer and R. K. Nelson (1997) Seasonal variation of CDOM and DOC in the Middle Atlantic Bight: terrestrial inputs and photooxidation. *Limnol. Oceanogr.* **42**, 674–686.
85. Vetter, R. D., A. Kurtzman and T. Mori (1999) Diel cycles of DNA damage and repair in eggs and larvea of northern anchovy, *Engraulis mordax*, exposed to solar ultraviolet radiation. *Photochem. Photobiol.* **69**, 27–33.
86. Nelson, N. B., D. A. Siegel and A. F. Michaels (1998) Seasonal dynamics of colored dissolved material in the Sargasso Sea. *Deep-Sea Res. I* **45**, 931–957.
87. Jagger, J. (1958) Photoreactivation. *Bacteriol. Rev.* **22**, 99–142.
88. Karentz, D. (1994) Ultraviolet tolerance mechanisms in Antarctic marine organisms. In *Ultraviolet Radiation in Antarctica: Measurements and Biological Effects*, Vol. 62 (Edited by C. S. Weiler and P. A. Penhale), pp. 93–110. American Geophysical Union, Washington.
89. Neale, P. J., A. T. Banaszak and C. R. Jarriel (1998) Ultraviolet sunscreens in *Gymnodinium sanguineum* (dinophyceae): mycosporine-like amino acids protect against inhibition of photosynthesis. *J. Phycol.* **34**, 928–938.
90. Cullen, J. J. and P. J. Neale (1997) Effect of UV on short-term photosynthesis of natural phytoplankton. *Photochem. Photobiol.* **65**, 264–266.
91. Aas, P., M. M. Lyons, R. Pledger, D. L. Mitchell and W. H. Jeffrey (1996) Inhibition of bacterial activities by solar radiation in nearshore waters and the Gulf of Mexico. *Aquat. Microb. Ecol.* **11**, 229–238.
92. Kaiser, E. and G. J. Herndl (1997) Rapid recovery of marine bacterioplankton activity after inhibition by UV radiation in coastal waters. *Appl. Environ. Microbiol.* **63**, 4026–4031.
93. Wilhelm, S. W. and R. E. H. Smith (2000) Bacterial carbon production in Lake Erie is influenced by viruses and solar radiation. *Can. J. Fish. Aquat. Sci.* **57**, 317–326.
94. Cullen, J. J. (1982) The deep chlorophyll maximum: comparing vertical profiles of chlorophyll a. *Can. J. Fish. Aquat. Sci.* **39**, 791–803.
95. Buma, A. G. J., A. H. Engelen and W. W. C. Gieskes (1997) Wavelength-dependent induction of thymine dimers and growth rate reduction in the marine diatom *Cyclotella* sp. exposed to ultraviolet radiation. *Mar. Ecol. Prog. Ser.* **153**, 91–97.
96. Veen, A., M. Reuvers and P. Rónçak (1997) Effects of acute and chronic UV-B exposure on a green alga: a continuous culture study using a computer-controlled dynamic light regime. *Plant Ecol.* **128**, 28–40.
97. Kobayashi, H., K. Sato, Y. Komatsu, H. Morioka, J. D. Stewart, T. Toshiki and E. Ohtsuka (1999) Effects of a high-affinity antibody fragment on DNA polymerase reaction near a (6-4) photoproduct site. *Photochem. Photobiol.* **69**, 226–230.
98. Cullen, J. J., P. J. Neale and M. P. Lesser (1992) Biological weighting function for the inhibition of phytoplankton photosynthesis by ultraviolet radiation. *Science* **258**, 646–650.